Exploiting HOPNO-dicopper center interaction to development of inhibitors for human tyrosinase

Elina Buitrago, Clarisse Faure, Marcello Carotti, Elisabetta Bergantino, Renaud Hardré, Marc Maresca, Christian Philouze, Nicolas Vanthuyne, Ahcène Boumendjel, Luigi Bubacco, et al.

Exploiting HOPNO-dicopper center interaction to development of inhibitors for human tyrosinase

Elina Buitrago,[a,b] Clarisse Faure,[a] Marcello Carotti,[c] Elisabetta Bergantino,[c] Renaud Hardré,[d] Marc Maresca,[d] Christian Philouze,[a] Nicolas Vanthuyne,[d] Ahcène Boumendjel,[b,1] Luigi Bubacco,[c] Amaury du Moulinet d'Hardemare,[a] Hélène Jamet,[a] Marius Réglier,[d] Catherine Belle[a]*

[a]University of Grenoble Alpes, CNRS-UGA UMR 5250, DCM, CS 40700, 38058 Grenoble Cedex 9, France; [b]University of Grenoble Alpes, CNRS-UGA UMR 5063, DPM CS 40700, 38058 Grenoble Cedex 9, France; [c]Department of Biology, University of Padova, Via Ugo Bassi 58b, 35121 Padova, Italy; [d]Aix Marseille University, CNRS, Centrale Marseille, iSm2, Marseille, France

* Corresponding author
E-mail address: catherine.belle@univ-grenoble-alpes.fr
[1]Present address: University of Grenoble Alpes, INSERM, LRB, 38000 Grenoble, France

Abstract

In human, Tyrosinase enzyme (TyH) is involved in the key steps of protective pigments biosynthesis (in skin, eyes and hair). The use of molecules targeting its binuclear copper active site represents a relevant strategy to regulate TyH activities. In this work, we targeted 2-Hydroxypyridine-*N*-oxide analogs (HOPNO, an established chelating group for the tyrosinase dicopper active site) with the aim to combine effects induced by combination with a reference inhibitor (kojic acid) or natural substrate (tyrosine). The HOPNO-MeOH (**3**) and the racemic amino acid HOPNO-AA compounds (**11**) were tested on purified tyrosinases from different sources (fungal, bacterial and human) for comparison purposes. Both

compounds have more potent inhibitory activities than the parent HOPNO moiety and display strictly competitive inhibition constant, in particular with human tyrosinase. Furthermore, **11** appears to be the most active on the B16-F1 mammal melanoma cells. The investigations were completed by stereospecificity analysis. Racemic mixture of the fully protected amino acid **10** was separated by chiral HPLC into the corresponding enantiomers. Assignment of the absolute configuration of the deprotected compounds was completed, based on X-ray crystallography. The inhibition activities on melanin production were tested on lysates and whole human melanoma MNT-1 cells. Results showed significant enhancement of the inhibitory effects for the (*S*) enantiomer compared to the (*R*) enantiomer. Computational studies led to an explanation of this difference of activity based for both enantiomers on the respective position of the amino acid group versus the HOPNO plane.

Keywords

Human Tyrosinase, Inhibitor development, Melanin, Dicopper center

1. Introduction

With an active site composed by a coupled binuclear copper core, Tyrosinase enzymes (Ty, EC 1.14.18.1) are widely distributed throughout microorganisms, plants and mammals. They belong to the type-3 family of the copper-containing enzymes [1,2]. The structural knowledge on tyrosinases are mostly based on X-ray diffraction data obtained from fungi [3,4], bacterial [5,6], insect [7] and plant [8,9] sources. All these structures revealed a classical type-3 center with copper-copper distances in the range 2.9-3.9 Å in the $Cu^{II}(OH)Cu^{II}$ (*met*) form with each copper ion coordinated by three histidine residues (Fig. 1A). The mechanism of action of Tys involves an initial transformation of its natural substrate, (*L*-tyrosine to *L*-3,4-dihydroxyphenylalanine (*L*-DOPA) and a subsequent oxidation of *L*-DOPA into *L*-DOPA quinone (Fig. 1D) for mammals tyrosinases). During the corresponding hydroxylation of phenol to catechol, the copper center is proposed to go through several states: the *oxy* form

(μ-ŋ^2: ŋ^2-peroxido) dicopper(II) state (Fig. 1B) and the reduced (*deoxy)* dicopper(I) form (Fig.1C). The resulting *L*-DOPA quinone progresses in a series of further reactions that leads to the formation of poly-aromatic colored and amorphous pigments responsible for the browning of fruits and vegetables. In mammals, tyrosinases and its associate production of melanin are responsible for the pigmentation of skin tissues, hair and iris of the eyes, providing color and protective pigments [10]. Melanin in the skin is produced by melanosomes, organelles located in the melanocytes founded in the basal layer of the epidermis [11].

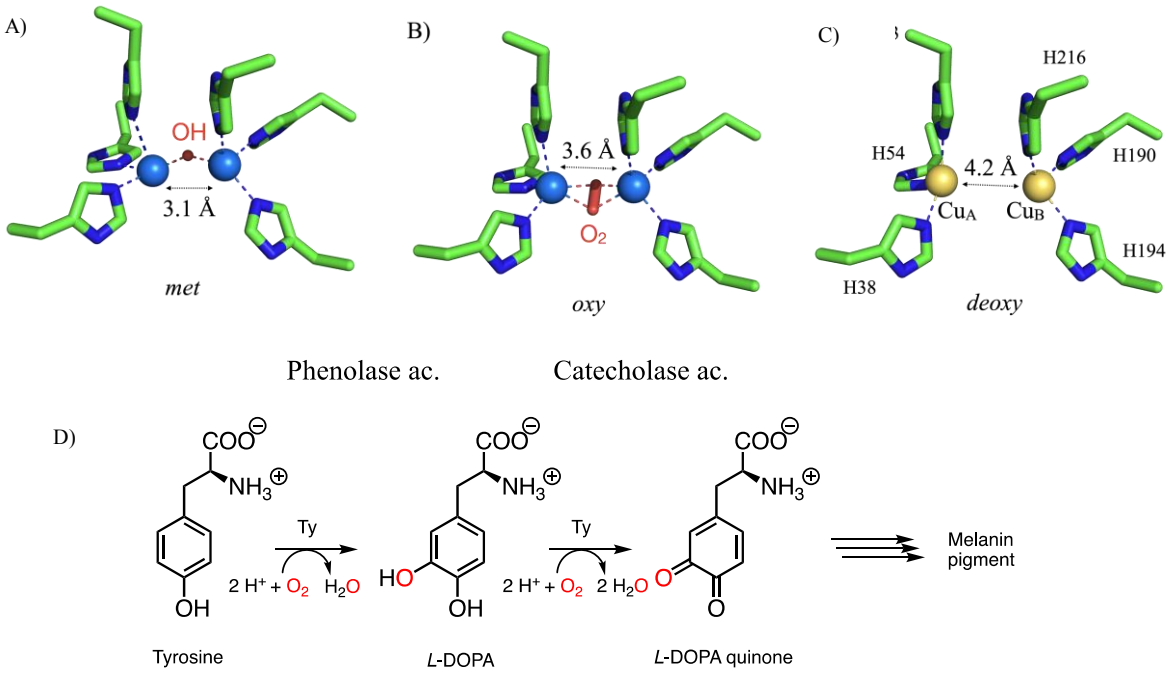

Figure 1. Structures of the active site of *Streptomyces castaneoglobisporus* Tyrosinase showing: (A) the dicopper(II) *met* form (PDB ID: 2ZMY); (B) the dicopper(II) *oxy* form (PDB ID: 1WX4) and C) the dicopper(I) *deoxy* form (PDB ID: 2AHL) that are involved in the catalysis. (D): Phenolase and catecholase activities of tyrosinase involved in the determining step of melanin pigments biosynthesis.

Associated tyrosinase enzymes (tyrosinase-related proteins -Trp1 and -Trp2) also take part in mammalian melanin biosynthesis [12]. The recently solved X-ray structure of Trp1 [13]

exhibited presence of a dinuclear zinc (in place of the expected di-copper) center and represents a breakthrough in the field of mammalian melanogenesis process despites unclarified functions associated to Trp1 [14]. In a normal setting, melanin plays a photoprotection role from exposure to UV radiation and consequentially skin cancer prevention (i.e. tanning after sun exposure) [15,16]. Additionally, melanin has antioxidant properties and is capable of neutralizing reactive oxygen species (ROS), such as hydroxyl radicals, superoxide or hydrogen peroxide [17,18]. Ty dysregulation is also involved in several skin diseases such as albinism, vitiligo (hypopigmentation) and melasma, linea nigra, smoker melanosis and melanoma (hyperpigmentation) [19]. Depigmenting agents are commonly prescribed in dermatology to treat disorders of hyperpigmentation but also widely used in cosmetic and nonprescription forms for skin lightening, [20–28] despite utilization of cytotoxic compounds as dihydroquinone. The product of dihydroquinone oxidation, benzoquinone, is a known mutagen and can damage DNA [29]. As a result of this and other side effects such as ochronosis [30,31] the use of dihydroquinone in cosmetics has been banned in the European Union (24th Dir. 2000/6/EC) and formulations are available only by prescription of physicians and dermatologists. Alternatives to dihydroquinone include arbutin (a natural β-glycoside of hydroquinone) and kojic acid (KA, 5-hydroxy-2-hydroxymethyl-4*H*-pyran-4-one (**1**), Scheme 1a) a well-studied inhibitor of tyrosinase used as benchmark. Unfortunately, neither substance offers a safe and effective alternative. Kojic acid is likely a carcinogen [32] while arbutin shares a toxicity profile with dihydroquinone [33]. In this context there is an urgent need for new strategies for the rational conception of Ty-inhibitors. In addition to efficiency of inhibition, other parameters related to solubility, skin and cellular penetration parameters should be considered.

Until now, efforts to develop inhibitors against Tys have largely been performed using non-human Tys (and particularly with the commercially available mushroom Ty) due to the

difficulties in expression and purification of TyHs, which is anchored to the membranes of melanosomes [34–37] and also to the lack of 3D structure of mammalian Tys. Alternatively homology modeling [12,38] or the recent AlphaFold AI approach [39] can be used instead of crystallographic data. Tys from different sources possess a similar dicopper active center [40,41] but the second coordination sphere of the metal ions in the active site (atoms within ~6 Å from the Cu ions) from multiple Tys displays low topological identity, suggesting differences in the binding pocket [42] in accordance with the resolved crystal structures mentioned above. Given this low identity, it is hard to correlate the observed inhibitory activities among the different Tys, which is a potential obstacle in translating inhibitor development into clinic trials.

Aiming to discover efficient Ty inhibitors, our strategy was to target directly the Ty binuclear copper center to generate competitive inhibitors where it binds dioxygen and provides two electrons to produce the oxygen active species (*oxy* form, Fig.1B) that will then react with the bound phenolic substrate. Blocking both dioxygen and substrate binding appears to be an efficient and rational strategy to maximize Ty inhibition. In this direction, we leveraged on the ability of HOPNO (2-hydroxypyridine-*N*-oxide or its corresponding tautomeric form as *N*-hydroxy-2-pyridone) motif (**2**), Scheme 1c) to coordinate the dicopper center as catechol does because of its structural analogies and non-oxidable structure that blocks the enzyme activity [43–45]. Since HOPNO exhibits Ty inhibition in the range of the micromolar concentrations on the human, bacterial and mushroom forms (see Table 1 and ref. [44]), it represents a good starting point for a pharmaco-modulation approach. We considered that the chemical modification of substrate/known inhibitor by introducing a HOPNO moiety able to bind the dicopper center is an important feature for the reinforcement of interactions with the active site [46] associated to supplementary benefits from additional skeletons to strengthen

inhibition properties and also selectivity for a given Ty source. This allowed us to recently identify that the attachment of HOPNO (Scheme 1c) to known inhibitors (aurones) resulted in an improvement of the inhibition activity on *Agaricus bisporus* Tyrosinase (TyAb) [47] and later on TyHs [48]. Consequently, this prompted others groups to develop some HOPNO-based inhibitors [49,50]. To confirm the interest of our approach we describe herein the embedding of 2-hydroxypyridine-*N*-oxide group in kojic acid as (HOPNO-MeOH, (**3**), Scheme 1d) and in the tyrosine (HOPNO-AA, (**11**), Scheme 1d). This methodology represents a potential path for a rational design of new inhibitors displaying an improved selectivity [46].

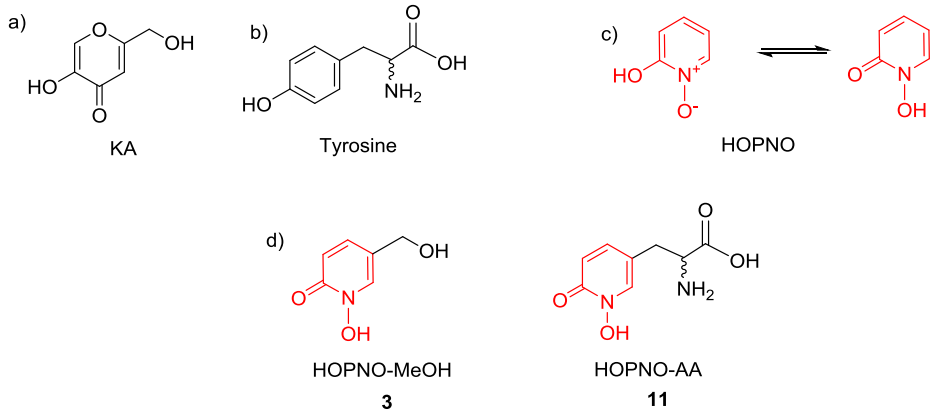

Scheme 1: a) Kojic acid; b) Tyrosine amino acid c) tautomeric forms of HOPNO; d) compounds synthetized in this work

2. Experimental

2.1. Material and methods. The solvents used for chemical reactions, electrochemistry and spectroscopic characterization were purified using the standard purification methods. Microanalysis was performed on an Elemental Thermo Finnigan EA 1112. Electrospray mass spectra were recorded on an Esquire 3000 plus Bruker Daltonics with nanospray inlet. A Unity Plus 400 MHz spectrometer was used for collection of NMR spectra. Microwave irradiation experiments were conducted in a CEM Discover S-Class apparatus (single mode

technology). Chiral HPLC analyses were achieved on a Lachrom-Elite unit with a Jasco CD-1595 detector. Optical rotations were measured on a 241 MC Perkin-Elmer polarimeter with a sodium lamp (589 nm), a mercury lamp (546, 436 and 365 nm) and a double-jacketed 10 cm cell at 25°C.

2.2. Synthesis

6-Methoxy-3-pyridinemethanol (5). 6-Methoxy-3-pyridinecarboxaldehyde (**4**) (500 mg, 1.03 mmol) was dissolved in MeOH (10 mL) and $NaBH_4$ (136 mg, 3.6 mmol) was added at 0°C. After completion, water (30 mL) was added to the solution and the product was extracted with CH_2Cl_2 (3x50 mL) to yield the product (**5**) as a colorless oil in 92% (465 mg, 3.3 mmol). ^{1}H-NMR (400 MHz, $CDCl_3$/d_6-DMSO) δ ppm: 8.11 (ds, 1H, J = 2.0 Hz), 7.62 (dd, 1H, J_1 = 2.4 Hz, J_2 = 8.5 Hz), 6.74 (d, 1H, J = 8.5 Hz), 4.61 (s, 2H), 3.94 (s, 3H); ^{13}C-NMR (100 MHz, $CDCl_3$/d_6-DMSO) δ ppm: 156.7, 137.6, 132.2, 126.5, 107.2, 59.9, 56.7.

6-Methoxy-3-pyridinemethanol-*N*-oxide (6). (465 mg, 3.3 mmol) of (**5**) was dissolved in CH_2Cl_2 (10 mL), mCPBA (1140 mg, 6.6 mmol) was added and the temperature was increased to reflux. When no more starting material was visible by TLC, the temperature was lowered to rt and the solvent was removed. The crude product was purified by column chromatography eluted with CH_2Cl_2:MeOH (9:1 to 8:2) to give the product (**6**) as a white solid in 75% yield (384 mg, 2.5 mmol). ^{1}H-NMR (400 MHz, $CDCl_3$/ d_6-DMSO) δ ppm: 8.17 (s, 1H), 7.61 (dd, 1H, J = 1.6 Hz, 8.7 Hz), 7.43 (s, 1H), 7.24 (d, 1H, J = 8.7 Hz), 4.58 (s, 2H), 3.97 (s, 3H). ^{13}C-NMR (100 MHz, $CDCl_3$/ d_6-DMSO) δ ppm: 156.7, 137.6, 132.2, 126.5, 107.2, 59.9, 58.7.

6-Pyridinone-3-methanol-*N*-hydroxy (3) (50 mg, 0.32 mmol) of (**6**) was dissolved in HCl (2M aq, 2 mL) and the solution was refluxed for 16 h. After lowering the temperature to ambient, the solvent was removed under reduced pressure to give HOPNO-MeOH (**3**) as a

yellow solid in 93 % yield (42 mg, 0.29 mmol). ^{1}H-NMR (400 MHz, d_6-DMSO): δ ppm 7.68 (s, 1H), 6.87 (d, 1H, J = 4.5 Hz), 6.14 (d, 1H, J = 8.6 Hz), 4.19 (s, 2H). ^{13}C-NMR (100 MHz, CD_3OD) δ ppm: 163.2, 138.0, 133.8, 122.0, 117.0, 62.1. MS (ESI) *m/z* 140 $(M-H)^-$.

***rac*-Methyl 2-(tert-butoxycarbonylamino)-3-(6-methoxy-3-pyridine-3-yl) acrylate (8).** Boc-protected phosphono glycine trimethyl ester (430 mg, 1.45 mmol) was dissolved in CH_2Cl_2 (6 mL). DBU (0.22 mL, 1.45 mmol) was added at 0°C followed by **4** (180 mg, 1.32 mmol). The reaction was stirred at rt for 16 h. Water (20 mL) was added to the mixture followed by HCl (1 M, 40 mL). The product was extracted with EtOAc (4x50 mL) and after drying with $MgSO_4$ the solvent was removed under reduced pressure. The crude product was purified by column chromatography to yield **8** as a white solid in 81% (365 mg, 1.18 mmol). ^{1}H-NMR (400 MHz, $CDCl_3$) δ ppm: 8.29 (d, 1H, J = 2.3 Hz), 7.84 (broad, 1H), 7.26 (s, 1H), 6.72 (d, 1H, J = 8.8 Hz), 6.25 (broad, 1H), 3.96 (s, 3H), 3.85 (s, 3H), 1.42 (s, 9H); ^{13}C-NMR (100 MHz, $CDCl_3$) δ ppm: 165.8, 164.1, 152.7, 149.2, 139.0, 127.3, 123.8, 110.9, 81.2, 53.8, 52.6, 28.1

***rac*-*N*-Boc-(6-Methoxypyridine-5-yl) alanine methyl ester (9). 8** (320 mg, 1.03 mmol) was dissolved in MeOH (5 mL). $NiCl_2{\cdot}6H_2O$ (245 mg, 1.03 mmol) was added followed by addition of $NaBH_4$ (340 mg, 9 mmol). When no more starting material remained brine (50 mL) was added to the solution and the product was extracted with Et_2O (4 × 50 mL) to yield the product **9** as a white solid in 78% (250 mg, 0.8 mmol). ^{1}H-NMR (400 MHz, $CDCl_3$) δ ppm: 7.88 (s, 1H), 7.32 (d, 1H, J = 8.5 Hz), 6.65 (d, 1H, J = 8.5 Hz), 5.05 (broad, 1H), 4.52 (broad, 1H), 3.88 (s, 3H), 3.7 (s, 3H), 3.07 (dd, 1H, J = 5.3 Hz, 14.1 Hz), 2.96 (dd, 1H, J = 5.8 Hz, 14.1 Hz), 1.38 (s, 9H); ^{13}C-NMR (100 MHz, $CDCl_3$) δ ppm: 171.9, 1633, 155.0, 147.0, 139.5, 124.2, 110.7, 80.0, 54.2, 53.3, 52.2, 34.7, 28.2

***rac*-*N*-Boc-(6-Methoxy-pyridine-N-oxide-5-yl) alanine methyl ester (10). 9** (100 mg, 0.32 mmol) was dissolved in CH_2Cl_2 (10 mL). mCPBA (220 mg, 1.27 mmol) was added and the

temperature was increased to reflux. After 24 h the temperature was lowered to rt and the solvent was removed. The crude product was purified by column chromatography (CH_2Cl_2:MeOH from 100:7 to 100:10) to give the product as a yellow oil in 72% yield (77 mg, 0.23 mmol). ^{1}H-NMR (400 MHz, $CDCl_3$) δ ppm: 8.13 (s, 1H), 7.17 (d, 1H, J = 8.5 Hz), 6.86 (d, 1H, J = 8.6 Hz), 5.16 (broad, 1H), 4.55 (broad, 1H), 4.07 (s, 3H), 3.76 (s, 3H), 3.09 (dd, 1H, J = 5.2 Hz, 14.2 Hz), 2.94 (dd, 1H, J = 6.5 Hz, 14.2 Hz), 1.42 (s, 9H); ^{13}C-NMR (100 MHz, $CDCl_3$/DMSO) δ ppm 171.3, 157.5, 155.0, 140.3, 130.7, 126.9, 107.9, 80.5, 57.4, 53.8, 52.8, 50.8, 34.7, 28.2. MS (ESI) *m/z* 327 $(M+H)^+$. Anal. Calculated for $C_{15}H_{22}N_2O_6 \cdot 0.45CH_3OH$: C 54.46, H 7.04, N 8.22, Found: C 54.18, H 7.21, N 8.52.

Racemic modified amino acid (11). The protected amino acid **10** (300 mg, 0.919 mmol) was solubilized in 9 ml of HCl (4M in water). The solution was heated at 130°C during one hour under microwave irradiations. Then, water was evaporated under reduce pressure and co-evaporated three times with toluene. 10 ml of EtOH were added to the crude product and heated to reflux (heterogeneous solution). After cooling, filtration and washing with Et_2O the desired deprotected product was obtained sufficiently pure as a white solid (186 mg, 0.793 mmol, 86% yield) as the hydrochloride salt form. ^{1}H NMR (400 MHz, MeOD) δ ppm: 7.87 (d, 1H),7.48 (d, 1H, J = 8.5 Hz), 6.69 (d, 1H, J = 9.0 Hz), 4.27 (t, 1H, J = 6.5 Hz), 3.08 (dq, 2H, J = 15.1 Hz, J = 5.7 Hz); ^{13}C NMR (100 MHz, D_2O) δ ppm: 171.6, 160.2, 141.8, 136.8, 120.0, 115.3, 53.9, 32.0. MS (ESI) *m/z* 199 $(M+H)^+$, 197 $(M-H)^-$, 233 $(M + Cl)^-$; Anal. Calculated for $C_8H_{10}N_2O_4 \cdot HCl$: C 40.94, H 4.73, N 11.94, Found: C 41.10, H 4.77, N 11.93.

2.3. Enantiomers separation.

Enantiomers separation of compound **10** was performed by preparative HPLC on chiral stationary phase: amylose *tris*(3,5-dimethyl-phenylcarbamate) immobilized on silica allowed an excellent baseline separation. Chiralpak IA (250 x 10 mm) was used to separate 1.5 g of

racemate, with heptane/ethanol/chloroform 30/50/20 as mobile phase: first fraction, ((+)-**10**): 725 mg, 48 % yield, ee > 99.5%; second fraction, ((-)-**10**): 713 mg of the second eluted fraction, 47 % yield, with ee > 99.5% (Details are in ESI).

Enantiomers for product **11** were synthesized according to the general procedure described for **11** using first fraction ((+)-**10**) or the second fraction ((-)-**10**) recovered from chiral separation of **10**.

(+)-11 was obtained as a white solid; ^{1}H NMR and ESI-MS are in ESI. Anal. calculated for $C_8H_{10}N_2O_4$·HCl: C 40.94, H 4.73, N 11.94, Found: C 41.23, H 4.95, N 11.78. HPLC analysis was done on an analytical Crownpak CR(+) column: mobile phase $HClO_4$ at pH = 1.3. The specific optical rotation (see ESI) was measured in MeOH.

(-)-11 was obtained as a white solid, ^{1}H NMR and ESI-MS are in ESI; Anal. calculated for $C_8H_{10}N_2O_4$·HCl: C 40.94, H 4.73, N 11.94, Found: C 40.86, H 4.95, N 11.81. HPLC analysis was done on an analytical Crownpak CR(+) column: mobile phase $HClO_4$ at pH = 1.3. The specific optical rotation (see ESI) was measured in MeOH.

2.4. Enzymes used in this study

A. bisporus Ty (TyAb, EC 1.14.18.1) used for the bioassay was purchased from Sigma (St. Louis, MO, USA) as a mixture of different polyphenol oxidases that was purified with Q-sepharose FF chromatography according to a described procedure [47]. *S. antibioticus* Ty (TySa) was prepared from liquid cultures of *S. antibioticus* harboring the pIJ703 expression plasmid and purified according to published procedure [51]. Human tyrosinase (TyH) was produced and purified as previously described [36,52].

2.5. Biological tests with bacterial, mushroom and human tyrosinases

Ty diphenolase activity was spectrophotometrically monitored with *L*-DOPA as the substrate at 25°C in phosphate buffer 100 mM, pH 7.2 by following the formation of dopachrome at a wavelength of 475 nm (ε = 3400 $M^{-1}cm^{-1}$) [53].

Typical assay on *A. bisporus and S. antibioticus Tys*: A microplate was charged with inhibitor and L-DOPA (0 to 10 mM) in phosphate buffer (50 mM with 2% DMSO). The enzyme was added to the mixture to initiate the reaction and the enzyme reaction was monitored by measuring the change in absorbance at 475 nm [40] of the DOPAchrome for 3 min at 25°C.

Typical assay on human tyrosinase: Inhibitors were dissolved in DMSO (final concentration of DMSO in the reaction mixture was 2%). The concentrations of *L*-DOPA employed ranged from 0.096 mM to 9.6 mM, and the concentrations of inhibitors tested ranged from 0.01 to 0.85 mM. The kinetic constants were determined in a 96-well plate assay, by using a SpectraMax 190 Absorbance Microplate Reader equipped with SoftMax 4.8 software or by using a single 100 mL quartz cell and the Agilent 8453 UV/Visible Spectroscopy System.

For all, the K_M and V_{max} values were calculated by fitting the obtained initial velocity (v_0) to the Michaelis–Menten equation, (Figures S12–S23 in the Supporting Information) using the KaleidaGraph software. The type of inhibitory mechanism against Ty during the oxidation of L-DOPA was determined by fitting the v_0 values obtained at different substrates and inhibitor concentrations to the equations describing different modes of inhibition, using the KaleidaGraph software. All measurements were done in triplicate, and the reported values are the mean and the standard error of at least three independent experiments.

2.6. B16-F1 melanoma cells melanin production assays. The effect of tyrosinase inhibitors on melanin synthesis was evaluated using the murine melanoma cell line B16-F1 which produce and secrete melanin, leading to a dark coloration of the cell media that could be easily quantified through optical density (OD) measurement at 600 nm. B16-F1 cells (passage number 20 to 40, obtained from Sigma Aldrich) were routinely grown in Dulbecco's

Modified Eagle Medium (DMEM) supplemented with 10% fetal calf serum (FCS), 1% *L*-glutamine and 1% antibiotics (all from Invitrogen, France) and maintained in a 5% CO_2 incubator at 37 °C. For studying inhibitor effects, B16-F1 cells were seeded at an initial density of 50,000 cells per wells in 96 well plates. After 24 h, inhibitors were directly added to the wells at the indicated final concentrations, control wells receiving the same volume of vehicle (*i.e.* 0.1% (v/v) of DMSO for HOPNO and 1% (v/v) of ethanol for kojic acid). Initial OD_{600nm} of the wells was measured using a BioTeck spectrophotometer. After 72 h of incubation in the 5% CO_2 incubator at 37 °C, the final OD_{600nm} of the wells was measured and the variation of OD_{600nm} was calculated by subtracting final and initial OD_{600nm} of each well.

2.7. Human MNT-1 melanoma cells melanin production assays.

Human melanoma cells (MNT-1) [54] were obtained from the National Institute of Health (NIH) and were grown in Dulbecco's Modified Eagle Medium F12 (DMEM-F12) supplemented with 10% fetal calf serum and 1% antibiotics, in a 75 cm^2 ventilated flask maintained at 37°C in a 5% CO_2 incubator. Cells were routinely passed by using trypsin-EDTA solution. Inhibition of tyrosinase by HOPNO-AAs and HOPNO compounds on MNT-1 was evaluated by using cell lysate prepared from MNT-1 cells. Briefly, confluent MNT-1 cells cultivated in 75 cm^2 flasks were washed with phosphate buffered saline (PBS) and detached by using a trypsin-EDTA solution. The cells suspension was aliquoted into cryotubes (approximately 4.10^{E6} cells per tube) and tubes were then centrifuged at 1200 rpm for 5 min. Supernatants were eliminated and cell pellets were snap-frozen in liquid nitrogen before being stored at -80°C until the tyrosinase assay. The day of the assay, tubes containing cell pellets were defrosted and cells were resuspended in 1.5 mL of PBS containing 0.1% Triton X-100. Tubes were incubated on ice for 10 min before being centrifuged at 1200 rpm for 5 min. Supernatants corresponding to MNT-1 cell extract were collected and used for the tyrosinase assay. Cell extracts were first diluted to 10 mL with PBS and then added to a 96-

well plate (100 µL per well). The test compounds (10 µL, diluted in DMSO) were next added to the wells and were serially diluted two times directly into the 96-well plate. Finally, 100 µL of a *L*-DOPA solution (initial concentration of 4 mM) was added into each well and the OD at 600 nm was immediately recorded (t_0 measurement). Plates were then incubated at 37°C, OD at 600 nm being continuously recorded until it reached OD ≈ 0.5 (about $t_f = t_0 + 3$ hours). Variation of OD_{600nm} was calculated (OD_{tf} - OD_{t0}) and used to determine IC_{50}. Inhibition of melanin synthesis by whole cells was performed as previously described [48]. MNT-1 cells grown on 75 cm^2 flask were detached using trypsin-EDTA solution and platted onto 6-wells plates at the initial density of 100,000 cells per cm^2. When cells reached confluence (typically after two to three days incubation at 37 °C in a 5% CO_2 incubator), MNT-1 cells were treated with increasing concentrations of test compounds for 96 h at 37 °C in a 5% CO_2 incubator. At the end of the incubation, cells were washed three times with cold PBS, scratched using rubber policemen and then transferred to Eppendorf tubes. After centrifugation (at 1,200 rpm for 5 min), cell pellets were finally lysed by adding 0.5 mL of NaOH (2 M) and repeated sonication / vortexing until melanin was completely solubilized. Cell-associated melanin contents were measured through reading of the absorbance of the samples at 600 nm. Pure melanin (purchased from Sigma-Aldrich) diluted in 2 M NaOH was used as standard for quantification. To allow normalization of the melanin concentrations, protein contents were determined using the Lowry's procedure, with bovine serum albumin (BSA) used as standard.

2.8. Computational methods

Geometry optimizations for the two possible configurations of the modified amino-acid **11** (*R* and *S*) were done with a deprotonated HOPNO motif and the zwitterionic state of the amino acid part. We used the hybrid functional B3LYP, the 6-31g* basis set on all atoms and the Gaussian09 package [55]. Vibrational frequency calculations were performed to ensure that

each geometry optimization converged to a real minimum. Docking calculations were done using the Autodock 4.2 software [56]. The input files for docking calculations were prepared with ADT Tools using Gasteiger partial charges for the enzyme. For the enantiomers of **11**, since we have anionic ligands, the charges were derived with a RESP fit on HF/6-31g* calculations. We used a homology model of human Tyrosinase [12] based on crystallographic structure of Trp1 (PDB: 5M8L) [13]. This choice is governed by the fact that this enzyme shares 70% of similarity with human Tyrosinase and also exhibits good interaction with known substrates of human Tyrosinase [13]. The model is taken in its *oxy* and *met* forms. For the *met* form, the two Cu ions (in place of Zn^{2+} ions in Trp1) and a hydroxo group (in place of the water molecule present in trp1 between the two Zn ions) were grafted to the homology model. For the *oxy* form, we used the geometry of the recent published *oxy* forms of the mushroom *A. oryzae* Tyrosinase (PDB code: 6JUC), [57]. Overlay of the used model with the one obtained with the AlphaFold AI approach [39] (AF-P14679-F1 model_v2) showing a high degree of similarity, is given in ESI (Fig. S26). The "AD4_parameters.dat" file in Autodock [58]was edited manually to include Cu ion parameters (an arbitrary charge of +2, Rii=3.50 Å, epsii = 0.005 kcal/mol and vol = 12 $Å^3$). A grid of 80 × 80 × 80 points centered on the active site and separated by 0.2 Å was used for the docking. A conformational search was performed using a genetic algorithm with an initial population of 300 randomly placed individuals, a maximum number of 2.5×10^5 energy evaluations, a maximum number of 2.7×10^4 generations, a mutation rate of 0.02, and a crossover rate of 0.8. One hundred different conformers of the ligand were generated and the energy values of conformers were reported as a histogram. The best rank position is taken as the docked position.

3. Results and discussions

3.1. Synthesis

The synthesis of HOPNO-MeOH (**3**) was achieved in three steps in 64% overall yield, according to Scheme 2. The aldehyde function of 6-methoxypyridine-3-carboxaldehyde **4** was reduced by means of $NaBH_4$ to yield the alcohol **5**. The latter was subjected to *N*-oxidation using *meta*-chloroperbenzoic acid (mCPBA) in CH_2Cl_2 which provided the corresponding *N*-oxide derivative **6**. Finally, intermediate **6** was demethylated in acidic conditions to yield the target compound **3** recovered in the pyridinone tautomeric form with 93% yield.

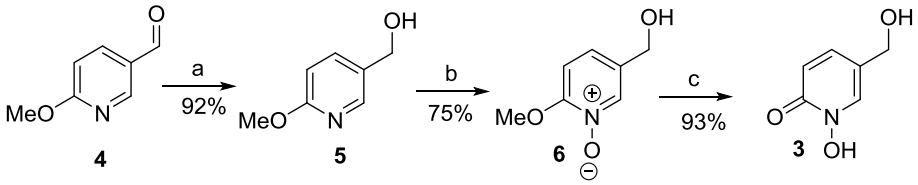

Scheme 2. a) $NaBH_4$, MeOH. b) mCPBA, CH_2Cl_2, reflux. c) HCl (aq, 2M).

Synthesis of the racemic modified amino acid HOPNO-AA (11)

The Boc-protected 2-methoxypyridine alanine methyl ester **9** (Scheme 3) was prepared by slight modifications of a reported procedure [59]. In short, the commercially available Boc-protected phosphonoglycine trimethyl ester **7** with 6-methoxy-3-pyridinecarboxaldehyde **4** yielded in presence of DBU the protected amino acid precursor **8**. Sodium borohydride reduction of the exocyclic double bond, in the presence of nickel(II) chloride, yielded the protected racemic amino acid **9**. The pyridine group of **9** was oxidized with mCPBA to give the *N*-oxide **10**. The methoxyl and Boc protecting groups were removed in a final deprotection with hydrochloric acid under microwave irradiations and provided **11** as the hydrochloride salt form with a yield of 86%.

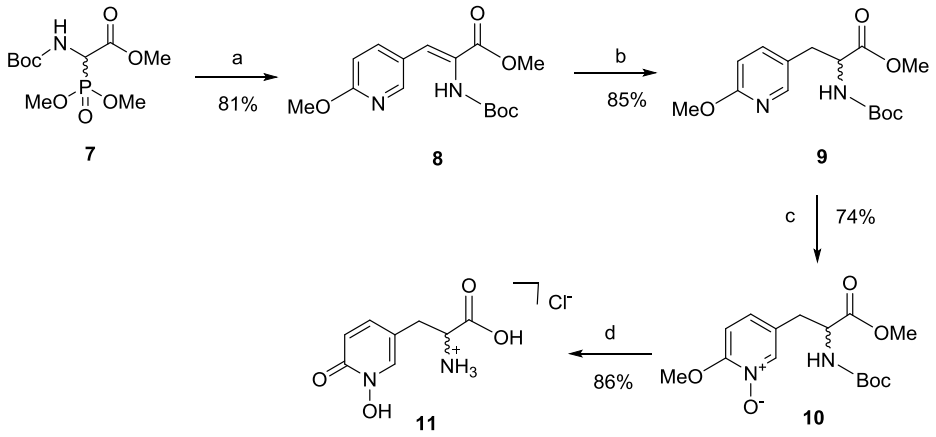

Scheme 3. Synthesis of the racemic amino acid HOPNO-AA (**11**): a) **4**, DBU, CH_2Cl_2; b) $NaBH_4$, $NiCl_2{\cdot}H_2O$, MeOH; c) mCPBA, CH_2Cl_2, reflux; d) HClaq, (4N), MW, 130°C, 1h

The analytical data of **11** are in accordance with a recently reported synthesis by a different way involving five steps from the commercially available compound **4** with an overall yield of 11% [60] whereas herein the synthesis of **11** was achieved in four steps and with a 44 % yield according to Scheme 3.

3.2 Comparative study between isolated tyrosinases (TyHs, TySa and TyAb) and melanin inhibition on mammal cells

In the present study the effects of compound **3** and **11** on the oxidation of *L*-DOPA by purified Ty from different sources (see details in the experimental part) were studied and compared to the value obtained from KA and HOPNO. We used the commercially available fungal source from *Agaricus bisporus* (TyAb); the bacterial from *Streptomyces antibioticus* (TySa) and recombinant human Ty from *Homo sapiens* (TyHs) produced in insect cells [36].

Furthermore, the *in vitro* activity was confirmed by measuring the melanogenesis suppression ability of the compounds in melanoma cells, i.e. B16-F1 murine model. B16-F1 cells produce, accumulate and secrete melanin (avoiding penetration parameters) as demonstrated by a

strong coloration (brown to black) of the cell media over time that could be measured at 600 nm (maximal OD after 72 h of culture, data not shown). Results are reported in Table 1 and in ESI.

Table 1: Effects of kojic acid, HOPNO and compounds **3** and **11**: comparison of the kinetic inhibition constants (K_I) obtained for tyrosinases from different sources: (TyAb); (TySa) and (TyHs) for competitive (C) and mixed (M) inhibition. For melanin inhibition on mammals B16-F1 cells, the IC_{50} value are reported.

	Murine B16-F1 melanoma cells	***H. sapiens* (TyHs)**		***S. antibioticus* (TySa)**		***A. bisporus* (TyAb)**	
Inhibitors	IC_{50} (μM)	K_I (μM)	type	K_I (μM)	type	K_I (μM)	type
Kojic Acid	108 ± 6	K_{IC} = 350 ± 10 K_{IU} = 730 ± 190 [36]	M	109 ± 5 [36]	C	102 [61]	C
HOPNO	19 ± 2	128 ± 2	C	7.7 ± 0.2 [43]	C	1.8 [44]	C
HOPNO-MeOH (3)	61.25	7.5 ± 0.5	C	4.1 ± 0.5	C	1.2 ± 0.3	C
HOPNO-AA (11)	10.03	6 ± 3	C	42 ± 3	C	1.2 ± 0.5	C

Embedding HOPNO moiety in KA or amino acid (AA), generated the "hybrid" compounds **3** and **11**, which showed an improvement of the inhibition activity for most of the isolated tyrosinases (excepted **11** on bacterial tyrosinase) with values comparable to the best inhibitors

described in literature. The effect is particularly evident on human tyrosinase with 20-fold lower competitive inhibition constant. Interestingly, the mixed inhibition behavior observed for KA on the human Ty only, is not detected with HOPNO-MeOH, HOPNO or HOPNO-AA, supported by the best chelating properties of HOPNO motif able to interact with dicopper centers [43,44].

The racemic HOPNO-AA compound appears to be the most active on the B16-F1 mammal melanoma cells. We therefore decided to complete the preliminary investigations with studies of the inhibition by HOPNO modified amino acid including studies on the stereospecificity. Data from published works (from mammal [62–67], bacterial [68–71] or fungal [72–77] tyrosinases) indicate that different chiral substrates show various degree of stereoselectivity on the activities / inhibition of the enzymes, but conflicting results from literature make to date the trends unreliable.

3.3 Enantiomers resolution of modified amino acid HOPNO-AA (11)

To investigate the stereospecificity, the enantiomers of **11** were separated. As **11** is recovered as a pure raw product, we choose to perform a chiral separation on the protected amino acid **10**, precursor of **11,** under the assumption that no racemization occurs during the final deprotection step (done in multiple runs). Details, chromatograms, chromatographic parameters and CD traces are given in the experimental part and in ESI. Chromatography of the isolated compound **10** on chiral HPLC column confirmed that **10** was a racemate (Fig. S3). The chromatograms of the collected enantiomers are on Fig. S4. The first eluted enantiomer showed a positive CD sign at 254 nm and was called (+)-**10** and the second eluted fraction was negative and corresponds to the (-)-**10** enantiomer.

This separation is followed for each fraction by the deprotection in acidic medium according to the synthetic conditions described for the deprotection of racemic amino acid **11**. The

resulting compounds are recovered as pure products. The ^{1}H NMR and ESI spectra agree with the proposed formulae as well as the elemental analysis (see experimental section and ESI). Each was analyzed on a chiral analytical HPLC column (see ESI). The first eluted product (Rt = 6.12 mn, $[\alpha]_{365}^{25}$ = - 18 (MeOH, c = 0.18)) appears to be the (-)-**11** enantiomer when the second eluted enantiomer (Rt = 16.79, $[\alpha]_{365}^{25}$ = + 27 (MeOH, c = 0.17) appears to be the (+)-**11** enantiomer. The optical rotation values (Table S3) are not measurable at 589 nm due to the low concentration (solubility in methanol is limited).

3.4 Assignment of the absolute configuration of modified amino acid enantiomers

Furthermore, crystals suitable for X-Ray analysis were obtained after slow evaporation of an aqueous solution of the first eluted enantiomer, allowing determination of the X-ray structure and the assignment of the absolute configuration as *R* to (-)-**11** enantiomer (details in ESI). The latter appears to be in the *N*-hydroxy-6-pyridinone tautomeric form.

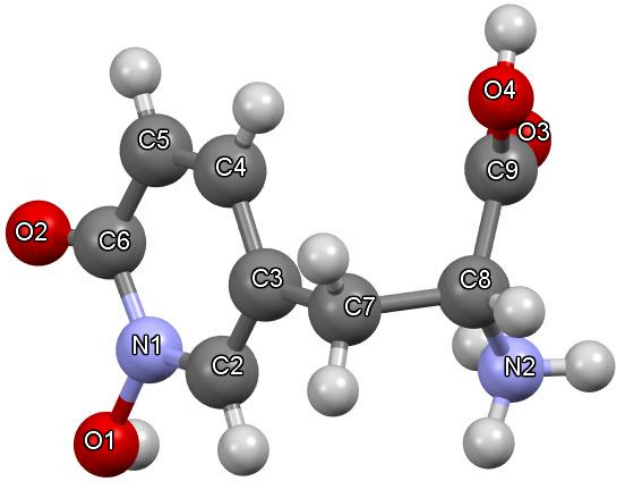

Figure 2. Representation of the X-ray structure of *R*-(-)-**11**·H_2O **(**$C_8H_{11}ClN_2O_4$·H_2O), the first eluted compound analyzed on a chiral analytical HPLC column with 50% probability thermal ellipsoids and partial atom labeling scheme. The Cl^- anion and the water molecule are omitted.

3.5. Evaluations of modified amino acids (racemic and enantiomers) for melanin biosynthesis inhibition.

Then to go further on the activity of presented modified amino acid (racemic and enantiomers), cellular assays on melanin biosynthesis suppression on human melanocytes cells (MNT-1, more accurate for human studies) were evaluated including studies on lysates and whole cells beside studies on isolated human tyrosinase. Table 2 reports the recorded values along those from on TyAb and TySa for comparison.

Table 2: Effects of modified amino-acids ((+)-**11**, (-)-**11** and racemic-**11**) with comparison of the kinetic inhibition constants (K_I) obtained for isolated tyrosinases ((TyAb), (TySa) and (TyHs)) for competitive (C) inhibition. For melanin inhibition on MNT-1 lysates and whole cells, the IC_{50} value are reported

	Human MNT-1		***H. sapiens* (TyHs)**		***S. antibioticus* (TySa)**		***A. bisporus* (TyAb)**	
	Lysates	**Whole cells**						
Inhibitors	IC_{50} (µM)	IC_{50} (µM)	K_I (µM)	type	K_I (µM)	type	K_I (µM)	type
HOPNO	1300 ± 100 [48]	200	128 ± 2[48]	C	7.7 ± 0.2 [43]	C	1.8 [44]	C
HOPNO-AA(±) (11)	90 ± 9	>> 400	6 ± 3	C	42 ± 3	C	1.2 ± 0.5	C
HOPNO-AA(+) ((+)-11)	73.6 ± 0.8	>> 400	8 ± 2	C	39 ± 2	C	12.5 ± 0.9	C
HOPNO-AA(-) ((-)-11)	277 ± 37	>> 400	76 ± 6	C	16 ± 4	C	12.8 ± 0.7	C

Surprisingly, on TyAb the inhibitory capacity of the racemic mixture was more effective (ten times) than the respective isolated pure enantiomers (both showed very similar $K_I \approx 12$ µM) at an equivalent concentration. This behavior could be explained by additional binding on the active site on TyAb leading to decrease the dissociation constant of the compounds as reported in others systems [45].

The bacterial enzyme showed no clear preference for racemic mixture displaying an inhibition constant slightly higher than the (+)-**11** whereas the best K_I value (16 ± 8 µM) was observed for the (-)-**11** with a value close to the one determined on TyAb (12.8 ± 0.7 µM). Conversely, with this last enantiomer, the human tyrosinase presented the worst inhibition whereas the (+)-enantiomer is the most efficient with value in the same range ($K_I \approx 6$ µM). The preference for (+)-**11** exhibited by the human tyrosinase was not reproduced on the bacterial or mushroom tyrosinase. These results point out that the active center (first and second coordination sphere) can recognize and discriminate between racemic/enantiomeric substrates. The spatial orientation of the modified amino acids can affect the interactions within the binding pocket and consequently the inhibition properties. To confirm this hypothesis, theoretical studies were performed (see part 3.6).

On the other hand, our data collected on human cells (lysates) showed that (+)-**11** displays better activity compared to (-)-**11** with a similar sequence of K_I or IC_{50} values: (+)-**11**< racemic-**11** < (-)-**11** than the one on the isolated TyH. Contribution of hybrid HOPNO-AA compounds in TyH inhibition is significant as the HOPNO alone had a very low activity on lysates. On the whole cells the IC_{50} value (>> 400 µM for all HOPNO-AA species) indicated a limited capacity to control melanogenesis. These results suggest a low ability to cross MNT-1 cell membranes for modified amino acids described in this work.

3.6. Docking Studies

Docking studies were undertaken to investigate the binding interactions of the two possible configurations of the modified amino-acid **11** with the *met* and the *oxy* forms of a human tyrosinase homology model (see experimental computational part). The *R* configuration was attributed to (-)-**11** enantiomer thanks to the X-ray structure of (-)-**11**·H_2O

($C_8H_{11}ClN_2O_4 \cdot H_2O$) (Fig. 2), and consequently the *S* configuration for the (+)-**11** enantiomer. Since the value of the protonation constant corresponding to a free HOPNO is 6.07 [45], the HOPNO motif of the two enantiomers is taken deprotonated. With the docking procedure, different positions were generated and structures close in positional root-mean-deviation (RMSD) were clustered together and ranked in a histogram according to their binding free energy. The docked positions obtained for the two enantiomers in the *met* and *oxy* form of the human tyrosinase are displayed in Figure 3. In both cases (*met* or *oxy* forms), they correspond to the best position of the lowest energy cluster and similar positions were obtained for the two enantiomers.

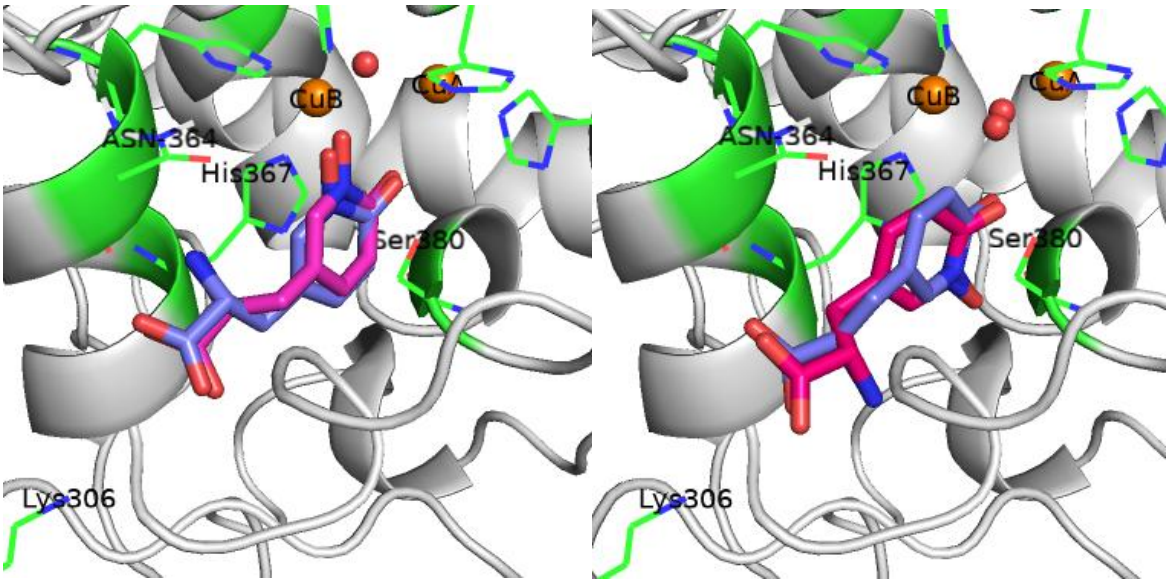

Figure 3. Left: Superposed docked positions obtained in the *met* form of a homology model of TyHs for the (+)-**11** (pink, (scoring function -5.25 kcal/mol, population: 78%)) and for (-)-**11** (purple) (scoring function -5.01 kcal/mol, population: 34%). Right: Superposed docked positions obtained in the *oxy* form of a homology model of TyHs for (+)-**11** (pink, (scoring function -4.96 kcal/mol, population: 63%)) and for (-)-**11** (purple) (scoring function -4.85 kcal/mol, population: 87%).

For the *met* form, both enantiomers of the deprotonated HOPNO motif interacted directly with the two copper atoms at a distance of 3.1 Å for CuB and 3.5 Å for CuA in (-)-**11** and for (+)-**11** 3.1Å with CuB and 3.0Å with CuA. This motif also formed a hydrogen bond between the oxygen atom of its hydroxyl group and Ser380 and interacted with His367 through aromatic stacking. This aromatic stacking interaction has already been described in X-ray structures of Tyrp1 with some substrates of human tyrosinase [12]. Hydrogen bonds appear between the amine group of the amino acid and the Asn364 residue, and between its carbonyl group with the Lys306 residue. For the *oxy* form, probably due to repulsive interaction with the peroxo group, the deprotonated HOPNO motif has shifted and the interaction between the oxygen atom of the nitrosyl and the copper atom (CuB) was lost. The hydrogen bond with Asn364 was also lost (Fig.3).

Even if same interactions were found between the two enantiomers and the human tyrosinase, for the *met* form the cluster is much more populated for **(+)-11** compared to **(-)-11**. The cluster associated to **(+)-11** contains 78 positions against 34 for to **(-)-11**. Moreover, the conformation adopted by the enantiomer in the active site is different, (-)-**11** being more constrained than **(+)-11**. Geometry optimization of the two enantiomers in water gives a value of the C4C3C7C8 dihedral angle with the notation of carbon atoms of the Figure 2 equal to -76° for (-)-**11** and -72° for (+)-**11**. In the docked position, this angle is equal to 177° for (-)-**11** and -88° for (+)-**11**. Thus, the conformation of (+)-**11** is less modified than those of (-)-**11** in the active site. This difference could rationalize the high activity of **(+)-11** compared to **(-)-11** in the human tyrosinase. For the *oxy* form, these differences of conformation are less pronounced (146° for (-)-**11** and -103° for (+)-**11**) and cluster for (-)-**11** is more populated, but the interactions are weaker. We can suppose that the difference of activity between the two enantiomers in the human tyrosinase is mostly due to their interactions with the *met* form.

4. Conclusion

The critical observation of the HOPNO moiety, a good metal chelator, together with kojic acid or human natural substrate (tyrosine) led us to propose new scaffolds which we hypotize could better target the Ty metal active site leading to a more selective and potent inhibitors. For comparison, inhibition ability has been tested on isolated tyrosinases from different sources (fungal, bacterial and human). All enzymes were found to produce the same quinone from the *L*-Dopa substrate, share a similar dinuclear active site but showed different features in terms of inhibition efficiency. On the other side, the poorly conserved second sphere of coordination between Tys of different origins has been already pointed as source of divergences for various inhibitors [36,40,77–80] in relation to variable binding pocket topologies and accessibility of the active site as illustrated in ESI (Fig. S27).

On human tyrosinase, the HOPNO-MeOH (**3**) and the racemic HOPNO-AA compound (**11**) have more potent inhibitory activities than the parent HOPNO moiety and display strictly competitive inhibition constant. Furthermore, **11** appears to be the most active on the B16-F1 mammal melanoma cells. The investigations were completed by stereospecificity analysis. The resolution of the racemic mixture of the protected modified amino acid **10** was performed by chiral HPLC allowing for the isolation of each enantiomer with good enantiopurity. The subsequent deprotection step allowed to obtain both HOPNO-AA enantiomers. The absolute configuration was established by X-Ray crystallographic analysis for enantiomer *R*(-)-**11** The three isolated tyrosinases tested in this work (fungal, bacterial and human) revealed completely different enantioselectivity for HOPNO-AA compounds. On human isolated tyrosinase enzyme and melanoma MNT-1 cells lysates, the best results in inhibition were performed by enantiomer *S*-(+)-**11**. The docking procedure on a TyH homology model (*met* and *oxy* forms) give similar positions for both and highlight interactions as π-π stacking with His367 and a hydrogen bond with Ser380 for the HOPNO motif. Conformations of the docked position for the two enantiomers in the *met* form were proposed to explain their

difference of activity, and more precisely the position of the amino acid group related to the HOPNO plane, measured with the C4C3C7C8 dihedral angle (Fig. 2).

In summary the integration of low molecular-weight chelating compound targeting the copper-center in tyrosinase in known inhibitor or substrate (this work) appears to be an important strategy for a rational design of new inhibitors displaying an improved selectivity. HOPNO-based compounds have already demonstrated very good ability to act in cell-based and physiological contexts.

Acknowledgment

The authors gratefully acknowledge the Labex Arcane (ANR-11-LABX-0003-01) with a grant for EB and Cosmethics project, an "Investissements d'Avenir" program (ANR-15-IDEX-02) with a grant for CF. The authors are grateful to ICMG UAR 2607 (PCN-ICMG) for the analytical facilities (NMR, ESI-MS, X-Ray) and to CECIC for computing facilities. This work has been partially supported by the CBH-EUR-GS (ANR-17-EURE-003) program, in the framework of which this work was carried out. The synthesis platform of DCM is acknowledged for providing large batch of compound **10** and **11** and Antonio García Jiménez for the help in cellular tests.

References

[1] E.I. Solomon, D.E. Heppner, E.M. Johnston, J.W. Ginsbach, J. Cirera, M. Qayyum, M.T. Kieber-Emmons, C.H. Kjaergaard, R.G. Hadt, L. Tian, Copper Active Sites in Biology, Chem. Rev. 114 (2014) 3659–3853. https://doi.org/10.1021/cr400327t.

[2] A. Bijelic, A. Rompel, C. Belle, Tyrosinases: Enzymes, Models and Related Applications, in: Ser. Chem. Energy Environ., World Scientific, 2019: pp. 155–183. https://doi.org/10.1142/9789813274440_0007.

[3] N. Fujieda, S. Yabuta, T. Ikeda, T. Oyama, N. Muraki, G. Kurisu, S. Itoh, Crystal Structures of Copper-depleted and Copper-bound Fungal Pro-tyrosinase, J Biol Chem. 288 (2013) 22128–22140. https://doi.org/10.1074/jbc.M113.477612.

[4] W.T. Ismaya, H.J. Rozeboom, M. Schurink, C.G. Boeriu, H. Wichers, B.W. Dijkstra, Crystallization and preliminary X-ray crystallographic analysis of tyrosinase from the mushroom *Agaricus bisporus*, Acta Crystallograph. Sect. F Struct. Biol. Cryst. Commun. 67 (2011) 575–578. https://doi.org/10.1107/S174430911100738X.

[5] Y. Matoba, T. Kumagai, A. Yamamoto, H. Yoshitsu, M. Sugiyama, Crystallographic Evidence That the Dinuclear Copper Center of Tyrosinase Is Flexible during Catalysis, J. Biol. Chem. 281 (2006) 8981–8990. https://doi.org/10.1074/jbc.M509785200.

[6] M. Sendovski, M. Kanteev, V. Shuster Ben-Yosef, N. Adir, A. Fishman, First Structures of an Active Bacterial Tyrosinase Reveal Copper Plasticity, J Mol Biol. 405 (2011) 227–237.

[7] Y. Li, Y. Wang, H. Jiang, J. Deng, Crystal structure of Manduca sexta prophenoloxidase provides insights into the mechanism of type 3 copper enzymes, Proc. Natl. Acad. Sci. 106 (2009) 17002. https://doi.org/10.1073/pnas.0906095106.

[8] A. Bijelic, M. Pretzler, C. Molitor, F. Zekiri, A. Rompel, The Structure of a Plant Tyrosinase from Walnut Leaves Reveals the Importance of "Substrate- Guiding Residues" for Enzymatic Specificity, Angew. Chem. Int. Ed. 54 (2015) 14677–14680. https://doi.org/10.1002/anie.201506994.

[9] I. Kampatsikas, A. Bijelic, M. Pretzler, A. Rompel, *In crystallo* activity tests with latent apple tyrosinase and two mutants reveal the importance of the mutated sites for polyphenol oxidase activity, Acta Crystallogr. Sect. F Struct. Biol. Commun. 73 (2017) 491–499. https://doi.org/10.1107/S2053230X17010822.

[10] M. d'Ischia, K. Wakamatsu, A. Napolitano, S. Briganti, J.-C. Garcia-Borron, D. Kovacs, P. Meredith, A. Pezzella, M. Picardo, T. Sarna, J.D. Simon, S. Ito, Melanins and melanogenesis: methods, standards, protocols, Pigment Cell Melanoma Res. 26 (2013) 616–633. https://doi.org/10.1111/pcmr.12121.

[11] J.D. Simon, D. Peles, K. Wakamatsu, S. Ito, Current challenges in understanding melanogenesis: bridging chemistry, biological control, morphology, and function, Pigment Cell Melanoma Res. 22 (2009) 563–579. https://doi.org/10.1111/j.1755-148X.2009.00610.x.

[12] X. Lai, H.J. Wichers, M. Soler-Lopez, B.W. Dijkstra, Structure and Function of Human Tyrosinase and Tyrosinase-Related Proteins, Chem. - Eur. J. 24 (2018) 47–55. https://doi.org/10.1002/chem.201704410.

[13] X. Lai, H.J. Wichers, M. Soler- Lopez, B.W. Dijkstra, Structure of Human Tyrosinase Related Protein 1 Reveals a Binuclear Zinc Active Site Important for Melanogenesis, Angew. Chem. Int. Ed. 56 (2017) 9812–9815. https://doi.org/10.1002/anie.201704616.

[14] H. Decker, F. Tuczek, The Recent Crystal Structure of Human Tyrosinase Related Protein 1 (HsTYRP1) Solves an Old Problem and Poses a New One, Angew. Chem. Int. Ed. 56 (2017) 14352–14354. https://doi.org/10.1002/anie.201708214.

[15] J.Y. Lin, D.E. Fisher, Melanocyte biology and skin pigmentation, Nature. 445 (2007) 843–850. https://doi.org/10.1038/nature05660.

[16] M. Brenner, V.J. Hearing, The Protective Role of Melanin Against UV Damage in Human Skin†, Photochem. Photobiol. 84 (2008) 539–549. https://doi.org/10.1111/j.1751-1097.2007.00226.x.

[17] G.J. Fisher, S. Kang, J. Varani, Z. Bata-Csorgo, Y. Wan, S. Datta, J.J. Voorhees, Mechanisms of Photoaging and Chronological Skin Aging, Arch. Dermatol. 138 (2002). https://doi.org/10.1001/archderm.138.11.1462.

[18] F.L. Meyskens Jr., P. Farmer, J.P. Fruehauf, Redox Regulation in Human Melanocytes and Melanoma, Pigment Cell Res. 14 (2001) 148–154. https://doi.org/10.1034/j.1600-0749.2001.140303.x.

[19] E. Buitrago, R. Hardré, R. Haudecoeur, H. Jamet, C. Belle, A. Boumendjel, L. Bubacco, M. Réglier, Are Human Tyrosinase and Related Proteins Suitable Targets for Melanoma Therapy?, Curr. Top. Med. Chem. 16 (2016) 3033–3047. https://doi.org/10.2174/1568026616666160216160112.

[20] T. Pillaiyar, M. Manickam, V. Namasivayam, Skin whitening agents: medicinal chemistry perspective of tyrosinase inhibitors, J. Enzyme Inhib. Med. Chem. 32 (2017) 403–425. https://doi.org/10.1080/14756366.2016.1256882.

[21] T. Pillaiyar, V. Namasivayam, M. Manickam, S.-H. Jung, Inhibitors of Melanogenesis: An Updated Review, J Med Chem. 61 (2018) 7395–7418. https://doi.org/10.1021/acs.jmedchem.7b00967.

[22] S.Y. Lee, N. Baek, T. Nam, Natural, semisynthetic and synthetic tyrosinase inhibitors, J Enzyme Inhib Med Chem. 31 (2016) 1–13. https://doi.org/10.3109/14756366.2015.1004058.

[23] G.-K. Agnieszka, P. Justyna, M. Henryk, Melanogenesis Inhibitors: Strategies for Searching for and Evaluation of Active Compounds, Curr. Med. Chem. 23 (2016) 3548–3574. http://dx.doi.org/10.2174/0929867323666160627094938.

[24] L. Panzella, A. Napolitano, Natural and Bioinspired Phenolic Compounds as Tyrosinase Inhibitors for the Treatment of Skin Hyperpigmentation: Recent Advances, Cosmetics. 6 (2019) 57. https://doi.org/10.3390/cosmetics6040057.

[25] P.G. Engasser, H.I. Maibach, Cosmetics and dermatology: Bleaching creams, J. Am. Acad. Dermatol. 5 (1981) 143–147. https://doi.org/10.1016/S0190-9622(81)70082-3.

[26] B. Roulier, B. Pérès, R. Haudecoeur, Advances in the Design of Genuine Human Tyrosinase Inhibitors for Targeting Melanogenesis and Related Pigmentations, J. Med. Chem. 63 (2020) 13428–13443. https://doi.org/10.1021/acs.jmedchem.0c00994.

[27] C. Couteau, L. Coiffard, Overview of Skin Whitening Agents: Drugs and Cosmetic Products, Cosmetics. 3 (2016) 27. https://doi.org/10.3390/cosmetics3030027.

[28] J. Li, L. Feng, L. Liu, F. Wang, L. Ouyang, L. Zhang, X. Hu, G. Wang, Recent advances in the design and discovery of synthetic tyrosinase inhibitors, Eur. J. Med. Chem. 224 (2021) 113744. https://doi.org/10.1016/j.ejmech.2021.113744.

[29] A. Begleiter, G.W. Blair, Quinone-induced DNA Damage and Its Relationship to Antitumor Activity in L5178Y Lymphoblasts, Cancer Res. 44 (1984) 78.

[30] P. Bhattar, V. Zawar, K. Godse, S. Patil, N. Nadkarni, M. Gautam, Exogenous Ochronosis, Indian J. Dermatol. 60 (2015) 537. https://doi.org/10.4103/0019-5154.169122.

[31] P. del Giudice, P. Yves, The widespread use of skin lightening creams in Senegal: a persistent public health problem in West Africa, Int. J. Dermatol. 41 (2002) 69–72. https://doi.org/10.1046/j.1365-4362.2002.01335.x.

[32] C.L. Burnett, W.F. Bergfeld, D.V. Belsito, R.A. Hill, C.D. Klaassen, D.C. Liebler, J.G. Marks, R.C. Shank, T.J. Slaga, P.W. Snyder, F.A. Andersen, Final Report of the Safety Assessment of Kojic Acid as Used in Cosmetics, Int. J. Toxicol. 29 (2010) 244S-273S. https://doi.org/10.1177/1091581810385956.

[33] SCCP (Scientific Comitee on Consumer Products), Opinion on beta-arbutin, European commission, 2008. https://ec.europa.eu/health/ph_risk/committees/04_sccp/docs/sccp_o_134.pdf. Accessed Mai 04,2022.

[34] N. Wang, D.N. Hebert, Tyrosinase maturation through the mammalian secretory pathway: bringing color to life, Pigment Cell Res. 19 (2006) 3–18. https://doi.org/10.1111/j.1600-0749.2005.00288.x.

[35] M.B. Dolinska, E. Kovaleva, P. Backlund, P.T. Wingfield, B.P. Brooks, Y.V. Sergeev, Albinism-Causing Mutations in Recombinant Human Tyrosinase Alter Intrinsic Enzymatic Activity, PLOS ONE. 9 (2014) e84494. https://doi.org/10.1371/journal.pone.0084494.

[36] S. Fogal, M. Carotti, L. Giaretta, F. Lanciai, L. Nogara, L. Bubacco, E. Bergantino, Human Tyrosinase Produced in Insect Cells: A Landmark for the Screening of New Drugs Addressing its Activity, Mol. Biotechnol. 57 (2015) 45–57. https://doi.org/10.1007/s12033-014-9800-y.

[37] X. Lai, M. Soler-Lopez, H.J. Wichers, B.W. Dijkstra, Large-Scale Recombinant Expression and Purification of Human Tyrosinase Suitable for Structural Studies, PLoS ONE. 11 (2016) e0161697. https://doi.org/10.1371/journal.pone.0161697.

[38] E. Favre, A. Daina, P.-A. Carrupt, A. Nurisso, Modeling the met form of human tyrosinase: a refined and hydrated pocket for antagonist design, Chem Biol Drug Des. 84 (2014) 206–215. https://doi.org/10.1111/cbdd.12306.

[39] J. Jumper, R. Evans, A. Pritzel, T. Green, M. Figurnov, O. Ronneberger, K. Tunyasuvunakool, R. Bates, A. Žídek, A. Potapenko, A. Bridgland, C. Meyer, S.A.A. Kohl, A.J. Ballard, A. Cowie, B. Romera-Paredes, S. Nikolov, R. Jain, J. Adler, T. Back, S. Petersen, D. Reiman, E. Clancy, M. Zielinski, M. Steinegger, M. Pacholska, T. Berghammer, S. Bodenstein, D. Silver, O. Vinyals, A.W. Senior, K. Kavukcuoglu, P. Kohli, D. Hassabis, Highly accurate protein structure prediction with AlphaFold, Nature. 596 (2021) 583–589. https://doi.org/10.1038/s41586-021-03819-2.

[40] R. Haudecoeur, A. Gouron, C. Dubois, H. Jamet, M. Lightbody, R. Hardré, A. Milet, E. Bergantino, L. Bubacco, C. Belle, M. Réglier, A. Boumendjel, Investigation of Binding-Site Homology between Mushroom and Bacterial Tyrosinases by Using Aurones as Effectors, ChemBioChem. 15 (2014) 1325–1333. https://doi.org/10.1002/cbic.201402003.

[41] M. Kanteev, M. Goldfeder, A. Fishman, Structure-function correlations in tyrosinases, Protein Sci. 24 (2015) 1360–1369. https://doi.org/10.1002/pro.2734.

[42] M. Pretzler, A. Rompel, What causes the different functionality in type-III-copper enzymes? A state of the art perspective, Inorganica Chim. Acta. 481 (2018) 25–31. https://doi.org/10.1016/j.ica.2017.04.041.

[43] C. Bochot, E. Favre, C. Dubois, B. Baptiste, L. Bubacco, P.-A. Carrupt, G. Gellon, R. Hardré, D. Luneau, Y. Moreau, A. Nurisso, M. Réglier, G. Serratrice, C. Belle, H. Jamet, Unsymmetrical Binding Modes of the HOPNO Inhibitor of Tyrosinase: From Model Complexes to the Enzyme, Chem. - Eur. J. 19 (2013) 3655–3664. https://doi.org/10.1002/chem.201202643.

[44] E. Peyroux, W. Ghattas, R. Hardré, M. Giorgi, B. Faure, A.J. Simaan, C. Belle, M. Réglier, Binding of 2-Hydroxypyridine- *N* -oxide on Dicopper(II) Centers: Insights into Tyrosinase Inhibition Mechanism by Transition-State Analogs, Inorg. Chem. 48 (2009) 10874–10876. https://doi.org/10.1021/ic901593x.

[45] M. Orio, C. Bochot, C. Dubois, G. Gellon, R. Hardré, H. Jamet, D. Luneau, C. Philouze, M. Réglier, G. Serratrice, C. Belle, The Versatile Binding Mode of Transition-State Analogue Inhibitors of Tyrosinase towards Dicopper(II) Model Complexes: Experimental and Theoretical Investigations, Chem. - Eur. J. 17 (2011) 13482–13494. https://doi.org/10.1002/chem.201100665.

[46] A.Y. Chen, R.N. Adamek, B.L. Dick, C.V. Credille, C.N. Morrison, S.M. Cohen, Targeting Metalloenzymes for Therapeutic Intervention, Chem. Rev. 119 (2019) 1323–1455. https://doi.org/10.1021/acs.chemrev.8b00201.

[47] C. Dubois, R. Haudecoeur, M. Orio, C. Belle, C. Bochot, A. Boumendjel, R. Hardré, H. Jamet, M. Réglier, Versatile Effects of Aurone Structure on Mushroom Tyrosinase Activity, ChemBioChem. 13 (2012) 559–565. https://doi.org/10.1002/cbic.201100716.

[48] R. Haudecoeur, M. Carotti, A. Gouron, M. Maresca, E. Buitrago, R. Hardré, E. Bergantino, H. Jamet, C. Belle, M. Réglier, L. Bubacco, A. Boumendjel, 2-Hydroxypyridine- *N* -oxide-Embedded Aurones as Potent Human Tyrosinase Inhibitors, ACS Med. Chem. Lett. 8 (2017) 55–60. https://doi.org/10.1021/acsmedchemlett.6b00369.

[49] D.-Y. Zhao, M.-X. Zhang, X.-W. Dong, Y.-Z. Hu, X.-Y. Dai, X. Wei, R.C. Hider, J.-C. Zhang, T. Zhou, Design and synthesis of novel hydroxypyridinone derivatives as potential tyrosinase inhibitors, Bioorg. Med. Chem. Lett. 26 (2016) 3103–3108. https://doi.org/10.1016/j.bmcl.2016.05.006.

[50] D.-F. Li, P.-P. Hu, M.-S. Liu, X.-L. Kong, J.-C. Zhang, R.C. Hider, T. Zhou, Design and Synthesis of Hydroxypyridinone-l-phenylalanine Conjugates as Potential Tyrosinase Inhibitors, J. Agric. Food Chem. 61 (2013) 6597–6603. https://doi.org/10.1021/jf401585f.

[51] L. Bubacco, E. Vijgenboom, C. Gobin, A.W.J.W. Tepper, J. Salgado, G.W. Canters, Kinetic and paramagnetic NMR investigations of the inhibition of Streptomyces antibioticus tyrosinase, J. Mol. Catal. B Enzym. 8 (2000) 27–35. https://doi.org/10.1016/S1381-1177(99)00064-8.

[52] E. Buitrago, C. Faure, L. Challali, E. Bergantino, A. Boumendjel, L. Bubacco, M. Carotti, R. Hardré, M. Maresca, C. Philouze, H. Jamet, M. Réglier, C. Belle, Ditopic Chelators of Dicopper Centers for Enhanced Tyrosinases Inhibition, Chem. – Eur. J. 27 (2021) 4384–4393. https://doi.org/10.1002/chem.202004695.

[53] H.S. Mason, The Chemistry of Melanin: III. Mechanism of the oxidation of Dihydroxyphenylalanine by Tyrosinase, J Biol Chem. 172 (1948) 83–99.

[54] K.G. Chen, R.D. Leapman, G. Zhang, B. Lai, J.C. Valencia, C.O. Cardarelli, W.D. Vieira, V.J. Hearing, M.M. Gottesman, Influence of Melanosome Dynamics on Melanoma Drug Sensitivity, J Natl Cancer Inst. 101 (2009) 1259–1271. https://doi.org/10.1093/jnci/djp259.

[55] Gaussian 09, Revision A.02, Gaussian, Inc., Wallingford CT, 2016.

[56] G.M. Morris, D.S. Goodsell, R.S. Halliday, R. Huey, W.E. Hart, R.K. Belew, A.J. Olson, Automated docking using a Lamarckian genetic algorithm and an empirical binding free energy function, J. Comput. Chem. 19 (1998) 1639–1662. https://doi.org/10.1002/(SICI)1096-987X(19981115)19:14<1639::AID-JCC10>3.0.CO;2-B.

[57] N. Fujieda, K. Umakoshi, Y. Ochi, Y. Nishikawa, S. Yanagisawa, M. Kubo, G. Kurisu, S. Itoh, Copper–Oxygen Dynamics in the Tyrosinase Mechanism, Angew. Chem. Int. Ed. 59 (2020) 13385–13390. https://doi.org/10.1002/anie.202004733.

[58] P. Durai, Y.-J. Ko, J.-C. Kim, C.-H. Pan, K. Park, Identification of Tyrosinase Inhibitors and Their Structure-Activity Relationships via Evolutionary Chemical Binding Similarity and Structure-Based Methods, Molecules. 26 (2021) 566. https://doi.org/10.3390/molecules26030566.

[59] M.P. Samant, C. Miller, D.J. Hong, S.C. Koerber, G. Croston, C.L. Rivier, J.E. Rivier, Synthesis and biological activity of GnRH antagonists modified at position 3 with 3-(2-methoxy-5-pyridyl)-alanine*: [AA3]degarelix analogs, J. Pept. Res. 65 (2008) 284–291. https://doi.org/10.1111/j.1399-3011.2005.00219.x.

[60] S. Kyriakou, M. Mitsiogianni, T. Mantso, W. Cheung, S. Todryk, S. Veuger, A. Pappa, D. Tetard, M.I. Panayiotidis, Anticancer activity of a novel methylated analogue of L-mimosine against an in vitro model of human malignant melanoma, Invest. New Drugs. 38 (2020) 621–633. https://doi.org/10.1007/s10637-019-00809-0.

[61] W. Yi, C. Dubois, S. Yahiaoui, R. Haudecoeur, C. Belle, H. Song, R. Hardré, M. Réglier, A. Boumendjel, Refinement of arylthiosemicarbazone pharmacophore in inhibition of mushroom tyrosinase, Eur. J. Med. Chem. 46 (2011) 4330–4335. https://doi.org/10.1016/j.ejmech.2011.07.003.

[62] Y.M. Chen, W. Chavin, Incorporation of tyrosine carboxyl groups and utilization of d-tyrosine in melanogenesis, Anal. Biochem. 27 (1969) 463–472. https://doi.org/10.1016/0003-2697(69)90060-8.

[63] B. Jergil, C. Lindbladh, H. Rorsman, E. Rosengren, Dopa oxidation and tyrosine oxygenation by human melanoma tyrosinase, Acta Derm. Venereol. 63 (1983) 468–475.

[64] A.J. Winder, H. Harris, New assays for the tyrosine hydroxylase and dopa oxidase activities of tyrosinase, Eur. J. Biochem. 198 (1991) 317–326. https://doi.org/10.1111/j.1432-1033.1991.tb16018.x.

[65] J. Park, H. Jung, K. Kim, K.-M. Lim, J. Kim, E. Jho, E.-S. Oh, D-tyrosine negatively regulates melanin synthesis by competitively inhibiting tyrosinase activity, Pigment Cell Melanoma Res. 31 (2018) 374–383. https://doi.org/10.1111/pcmr.12668.

[66] S. Ito, W. Gerwat, L. Kolbe, T. Yamashita, M. Ojika, K. Wakamatsu, Human tyrosinase is able to oxidize both enantiomers of rhododendrol, Pigment Cell Melanoma Res. 27 (2014) 1149–1153. https://doi.org/10.1111/pcmr.12300.

[67] S.H. Pomerantz, Separation, Purification, and Properties of Two Tyrosinases from Hamster Melanoma, J. Biol. Chem. 238 (1963) 2351–2357.

[68] S. Molloy, J. Nikodinovic-Runic, L.B. Martin, H. Hartmann, F. Solano, H. Decker, K.E. O'Connor, Engineering of a bacterial tyrosinase for improved catalytic efficiency towards D-tyrosine using random and site directed mutagenesis approaches, Biotechnol. Bioeng. 110 (2013) 1849–1857. https://doi.org/10.1002/bit.24859.

[69] V. Shuster, A. Fishman, Isolation, Cloning and Characterization of a Tyrosinase with Improved Activity in Organic Solvents from *Bacillus megaterium*, J. Mol. Microbiol. Biotechnol. 17 (2009) 188–200. https://doi.org/10.1159/000233506.

[70] H. Yoshida, Y. Tanaka, K. Nakayama, Properties of Tyrosinase from Pseudomonas melanogenum, Agric. Biol. Chem. 38 (1974) 627–632. https://doi.org/10.1080/00021369.1974.10861206.

[71] M. Ito, K. Oda, An Organic Solvent Resistant Tyrosinase from Streptomyces sp. REN-21: Purification and Characterization, Biosci. Biotechnol. Biochem. 64 (2000) 261–267. https://doi.org/10.1271/bbb.64.261.

[72] J.L. Muñoz-Muñoz, J.R. Acosta-Motos, F. Garcia-Molina, R. Varon, P.A. Garcia-Ruíz, J. Tudela, F. Garcia-Cánovas, J.N. Rodríguez-López, Tyrosinase inactivation in its action on dopa, Biochim. Biophys. Acta BBA - Proteins Proteomics. 1804 (2010) 1467–1475. https://doi.org/10.1016/j.bbapap.2010.02.015.

[73] P.J. Fernandez- Julia, J. Tudela- Serrano, F. Garcia- Molina, F. Garcia- Canovas, A. Garcia- Jimenez, J.L. Munoz- Munoz, Study of tyrosine and dopa enantiomers as tyrosinase substrates initiating L- and D- melanogenesis pathways, Biotechnol. Appl. Biochem. (2020) bab.1998. https://doi.org/10.1002/bab.1998.

[74] H.J. Martin, I. Kampatsikas, R. Oost, M. Pretzler, E. Al-Sayed, A. Roller, G. Giester, A. Rompel, N. Maulide, Total Synthesis, Stereochemical Assignment, and Divergent Enantioselective

Enzymatic Recognition of Larreatricin, Chem. - Eur. J. 24 (2018) 15756–15760. https://doi.org/10.1002/chem.201803785.

[75] D.E. Wilcox, A.G. Porras, Y.T. Hwang, K. Lerch, M.E. Winkler, E.I. Solomon, Substrate analog binding to the coupled binuclear copper active site in tyrosinase, J. Am. Chem. Soc. 107 (1985) 4015–4027. https://doi.org/10.1021/ja00299a043.

[76] J.C. Espín, P.A. García-Ruiz, J. Tudela, F. García-Cánovas, Study of stereospecificity in mushroom tyrosinase, Biochem. J. 331 (1998) 547–551. https://doi.org/10.1042/bj3310547.

[77] E. Selinheimo, D. NiEidhin, C. Steffensen, J. Nielsen, A. Lomascolo, S. Halaouli, E. Record, D. O'Beirne, J. Buchert, K. Kruus, Comparison of the characteristics of fungal and plant tyrosinases, J Biotech. 130 (2007) 471–480. https://doi.org/10.1016/j.jbiotec.2007.05.018.

[78] B. Deri, M. Kanteev, M. Goldfeder, D. Lecina, V. Guallar, N. Adir, A. Fishman, The unravelling of the complex pattern of tyrosinase inhibition, Sci. Rep. 6 (2016) 34993. https://doi.org/10.1038/srep34993.

[79] T.F.M. Kuijpers, T. van Herk, J.-P. Vincken, R.H. Janssen, D.L. Narh, W.J.H. van Berkel, H. Gruppen, Potato and Mushroom Polyphenol Oxidase Activities Are Differently Modulated by Natural Plant Extracts, J. Agric. Food Chem. 62 (2014) 214–221. https://doi.org/10.1021/jf4043375.

[80] T. Mann, W. Gerwat, J. Batzer, K. Eggers, C. Scherner, H. Wenck, F. Stäb, V.J. Hearing, K.-H. Röhm, L. Kolbe, Inhibition of Human Tyrosinase Requires Molecular Motifs Distinctively Different from Mushroom Tyrosinase, J. Invest. Dermatol. 138 (2018) 1601–1608. https://doi.org/10.1016/j.jid.2018.01.019.